Green Chemistry

PAPER

View Article Online
View Journal | View Issue

Cite this: *Green Chem.*, 2024, **26**, 2592

Preparation of reusable copper-based biomass-carbon aerogel catalysts and their application in highly selective reduction of maleimides to succinimides with hydrosilane as a hydrogen source†

Shaohuan Lv,‡[a] Zhanhong Yuan,‡[b,c] Juanjuan Zheng,[a] Zirong Liu,[b,c] Jiawang Ye,[a] Jiefang Li,[a] Shanshan Xu,[a] Feng Xie,[a] Dongdong Ye *[b,c] and Bin Li *[a,d]

Received 30th November 2023,
Accepted 29th December 2023

DOI: 10.1039/d3gc04697d

rsc.li/greenchem

Selective reduction is one of the most essential and frequently used transformations in organic synthesis. In this work, we developed a novel copper-based biomass-carbon aerogel catalyst ($Cu(OTf)_2$@CAC) as a highly efficient and selective catalyst for maleimide reduction with hydrosilane as a hydrogen source for the first time. A strategy integrating chitin dissolution, nanofibrous regeneration, aerogel construction, and customizable carbonization was designed for the reduction of copper trifluoromethane sulfonate ($Cu(OTf)_2$) to Cu(0) and Cu(I) on the CAC. The $Cu(OTf)_2$@CAC exhibited excellent catalytic activity, chemo-selectivity, and recyclability for selective maleimide reduction to succinimides under mild conditions. Moreover, the $Cu(OTf)_2$@CAC can be reused six times without noticeably losing activity. This work provides a representative and referential approach to achieve efficient catalytic conversion based on the reprocessing and customizable treatment of waste biomass resources.

Introduction

Developing efficient synthetic strategies for highly selective reduction reactions is essential due to their widespread occurrence in molecular synthesis.[1] Succinimides[2] are important structural units existing in natural products, pharmaceuticals, and advanced materials, such as *methsuximide*,[3] *moiramide B* and *andrimide*,[4] XCF-37B,[5] *etc.* (Fig. 1). Compared to the classical synthetic methodologies, selective reduction of maleimide is a straightforward method to synthesize functional succinimides owing to atom- and step-economy. With mild conditions and good chemoselectivities, hydrosilane has emerged as a suitable hydrogen donor for selective reduction[6] compared to the classical hydrogen[7] and metal hydride reagents (such as $LiAlH_4$ or $NaBH_4$).[8] However, most selective hydrosilylations to access target compounds using homogeneous transition metal catalysts require high catalyst loadings and ligands and cannot be reused. Maleimide comprising two –NCO– bonds and one C=C bond has attracted attention as a useful intermediate in organic transformations.[9] At least three reduction products would be produced *via* homogeneous transition metal-catalyzed reduction, including pyrrolidine, pyrrole, and succinimide.[10] The highly selective reduction to access succinimides is still a challenging issue that has to be solved.

Considering the above challenges, the development of recyclable catalysts would be the key to achieving the synthetic purpose. In recent years, owing to their high stability, easy

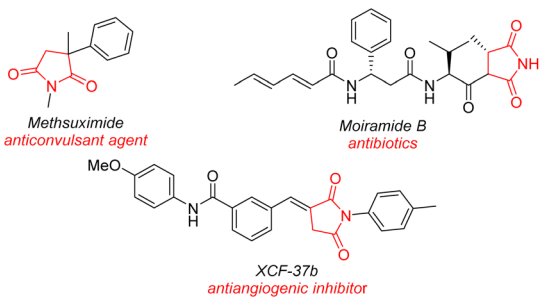

Fig. 1 Representative bioactive compounds bearing a succinimide fragment.

[a]*School of Environmental and Chemical Engineering, Wuyi University, Jiangmen 529020, Guangdong Province, China. E-mail: andonlee@163.com*
[b]*College of Light Textile Engineering and Art, Anhui Agricultural University, Hefei, Anhui 230036, China. E-mail: ydd@whu.edu.cn*
[c]*Biomass Molecular Engineering Center, Anhui Agricultural University, Hefei, Anhui 230036, China*
[d]*Jiangmen Key Laboratory of Synthetic Chemistry and Cleaner Production, Wuyi University, Jiangmen 529020, China*

†Electronic supplementary information (ESI) available. See DOI: https://doi.org/10.1039/d3gc04697d

‡These authors contributed equally to this work.

recyclability, and different pathways, heterogeneous metal nanocatalysts have obtained more and more attention in organic transformations,[11] such as CO_2 transformations,[12] Alder–ene reaction of allenynamides,[13] alcohol oxidation,[14] reductive amination,[15] nitrile reduction,[16] N-heterocycle synthesis,[17] *etc*.

Following our previous contributions on heterogeneous catalysis,[18] we wish to report herein the preparation of copper-based biomass-carbon aerogel catalysts ($Cu(OTf)_2$@CAC) and demonstrate their first application in the highly selective catalytic reduction of maleimides to achieve succinimides with hydrosilane as a hydrogen source under mild conditions. For the conversion of copper trifluoromethane sulfonate ($Cu(OTf)_2$) to Cu(0) and Cu(I) on the CAC, a method incorporating waste chitin (shrimp and crab shells) dissolution, nanofibrous regeneration, aerogel fabrication, and adaptable carbonization was developed. Under benign conditions, the $Cu(OTf)_2$@CAC showed outstanding chemo-selectivity, catalytic activity, and recyclability for selective maleimide reduction to succinimides. The $Cu(OTf)_2$@CAC can also be used up to 6 times without significantly losing effectiveness. Based on the reprocessing and adaptable treatment of waste biomass resources, this study offers a representative and reference strategy for effective catalytic conversion.

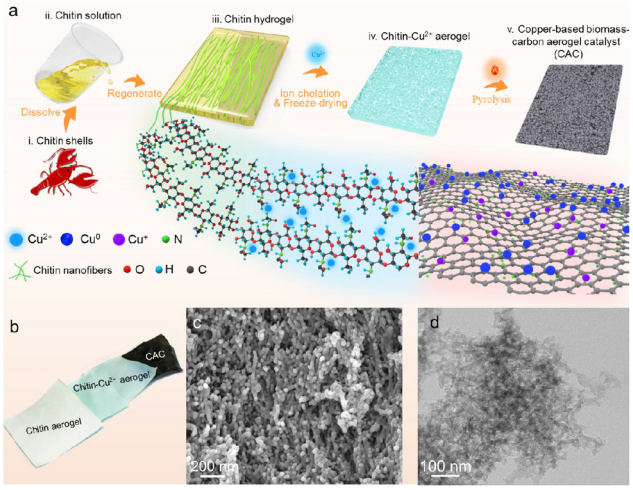

Fig. 2 (a) Schematic diagram of the preparation of the copper-based biomass carbon aerogel catalyst ($Cu(OTf)_2$@CAC). (b) Photographs of chitin aerogels, chitin/Cu^{2+} composite aerogels, and aerogel catalysts. (c) SEM image of $Cu(OTf)_2$@CAC. (d) High magnification TEM image of $Cu(OTf)_2$@CAC.

Results and discussion

Formation of a copper-based biomass-carbon aerogel catalyst ($Cu(OTf)_2$@CAC)

In this work, we designed a bottom-up approach by integrating chitin dissolution, regeneration, aerogel structuring, and pyrolysis to prepare a nanostructured copper-based biomass carbon aerogel catalyst ($Cu(OTf)_2$@CAC) (Fig. 2a). First, crab shells (Fig. S1, ESI†), which were purified as in our previous work,[18a] were dissolved using potassium hydroxide/urea solution to obtain a yellow, transparent and viscous chitin solution (Fig. S2†). Then, the chitin solution was subsequently poured into a customized mold, immersed in anhydrous ethanol to trigger the sol–gel phase transition and washed to obtain nanofibrous chitin hydrogels (Fig. S3†). Subsequently, ethanol and acetone were used alternately to remove the solvent in the gel, and the as-prepared organogel was immersed in $Cu(OTf)_2$-containing acetone solution to promote the stable complexation of Cu^{2+} with hydroxyl groups and amides on the molecular chain of chitin (Fig. S4†). Next, chitin-Cu^{2+} aerogels with three-dimensional porous structures were prepared by freeze-drying the above organogels. Finally, the CAC aerogel comprised Cu(0) and Cu(I), and the biomass carbon was prepared by pyrolyzing the composite aerogel under a nitrogen atmosphere (Fig. 2b). The SEM image shows a rich three-dimensional nano-network structure inside the copper-based biomass catalyst (Fig. 2c). Furthermore, the TEM images show that the chitin nanofibers present an amorphous nano-morphology after carbonization and realize the reduction of Cu^{2+} during the thermal decomposition process (Fig. 2d). The HRTEM images of Fig. S5† exhibited lattice fringes displaying interplanar spacings of 0.24 nm and 0.18 nm, being in agreement with Cu_3N(100) and Cu(100), respectively (Fig. S5†).[19] In addition, elements such as C, N, and Cu are shown using the EDS test. After carbonization, they are still retained and uniformly dispersed inside the $Cu(OTf)_2$@CAC specimen (Fig. S6†). The porous nanostructure and uniform element distribution of the $Cu(OTf)_2$@CAC specimen prove the feasibility of the strategy of using a chitin nanofibrous aerogel to support Cu, and at the same time provide abundant active sites for the improvement of catalytic activity.

We further explored the structural regulation process of the $Cu(OTf)_2$@CAC aerogel to reveal the effect of carbonization time on the microscopic morphology and determine the preparation conditions (Fig. 3). Raman imaging technology is a non-destructive and efficient method for characterizing material structures. We first tested the standard Raman spectra of the aerogel in different states (Fig. 3a). Obviously, the chitin/Cu(II) aerogel sample not only retains the C=O stretching vibration peak (1655.8 cm^{-1}) and the C–N out-of-plane bending vibration peak (953.0 cm^{-1}) of chitin, but also reserves the characteristics of metal salt peaks (750 and 1150 cm^{-1}).[20] Subsequently, the characteristic peaks of 1362.5 cm^{-1} and 1575.5 cm^{-1} in the Raman spectrum of the carbonized composite carbon aerogel represent the D and G peaks of amorphous carbon,[21] respectively. In contrast, the characteristic peaks of chitin completely disappear (Fig. 3b and Fig. S7†). Fig. 3c shows a representative line diagram of the Raman characteristic spectrum of the $Cu(OTf)_2$@CAC aerogel section treated with different carbonization times. The results show a strong time dependence of the D and G peak intensities from the surface to the interior of the carbon aerogel. When the pyrolysis time is less than 4 h, although the carbonization reaction

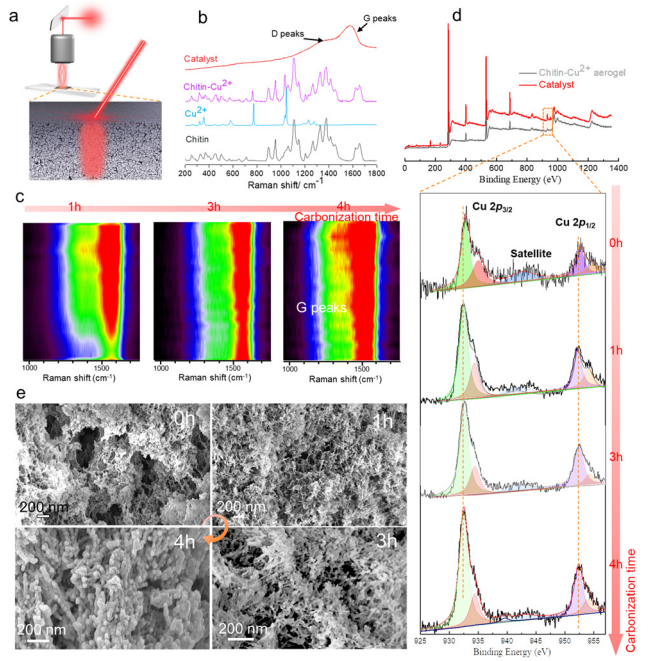

Fig. 3 Preparation parameters and structure of the CAC aerogel. (a) Schematic illustration of structural characterization by the Raman imaging technique. (b) Raman spectra of the CAC aerogel, chitin/Cu^{2+} aerogel, and pristine chitin aerogel. (c) Representative 2D Raman imaging from the outside to the inside of the composite aerogel treated with different pyrolysis times (0–4 h). (d) XPS spectra of composite carbon aerogels, chitin/Cu aerogels, and Cu 2p spectra after 0 h, 1 h, 3 h, and 4 h of carbonization. (e) SEM images of aerogels with different carbonization treatment times.

occurs inside the $Cu(OTf)_2$@CAC, the intensity of the D and G peaks is much lower than that on the surface; in contrast, when the pyrolysis time reaches 4 h, there is a uniform intensity distribution inside and outside the $Cu(OTf)_2$@CAC (Fig. 3c).

Furthermore, we used X-ray photoelectron spectroscopy (XPS) to detect the valence state changes of copper in the CAC prepared at different pyrolysis times to clarify the relationship between the chemical properties of the CAC and the carbonization time (Fig. 3d). As shown, there are representative peaks of Cu $2p_{3/2}$ (934.99 eV) and Cu $2p_{1/2}$ (954.85 eV), and a satellite peak of 941.01 eV in the chitin/Cu(II) aerogel, confirming the presence of solid chelation between chitin and Cu(II) for the retention of Cu(II).[22] After pyrolysis treatment, the characteristic peaks of Cu $2p_{3/2}$ and Cu $2p_{1/2}$ shifted to the direction of lower binding energies to 932.48 eV and 952.48 eV, respectively, indicating that Cu(II) was transformed into Cu(0) at a high-temperature pyrolysis process. In addition, the representative peaks of Cu–N at 934.38 eV and 954.08 eV also demonstrate the presence of Cu(I),[23–25] which is consistent with the interplanar spacing results. In addition, by prolonging the pyrolysis time from 1 h to 4 h, the Cu $2p_{3/2}$ and Cu $2p_{1/2}$ peak intensities continued to increase, proving the necessity of prolonging the pyrolysis time to increase the content of Cu(0) in the CAC. Besides, the peak intensity of N 1s also becomes lower than the pristine state, which testifies to the combination of Cu–N (Fig. S2†). Therefore, we set the pyrolysis time as 4 h. Subsequently, we characterized the microstructure of the composite aerogel with different pyrolysis times. The results showed that after pyrolysis treatment for 1 h, the microstructure of the aerogel still showed a uniform three-dimensional nanofiber network structure similar to the pristine aerogel, with a specific surface area and an average pore diameter of 135.2 $m^2\ g^{-1}$ and 32 nm, respectively; when the pyrolysis time was prolonged, the decomposition of chitin in the $Cu(OTf)_2$@CAC is more thorough, forming a denser nanonetwork structure (average pore size 12–22 nm) (Fig. 3e), and a maximum specific surface area of 152.5 $m^2\ g^{-1}$ (Fig. S9†). The above results illustrate that the timely pyrolysis process can achieve complete carbonization of the chitin nanofiber network and realize the reduction preparation of Cu(0) and Cu_3N. This carbon aerogel with a rich nanoporous structure is expected to achieve highly efficient catalytic effects.

Catalytic reduction of maleimides with hydrosilane

To test our hypothesis, we initially investigated the reaction of *N*-phenylmaleimide **1a** by using H_3SiPh as the hydrogen donor and 5 mol% of different ruthenium complexes, including $RuHCl(CO)(PPh_3)_3$, $Ru_3(CO)_{12}$, $RuH_2(CO)(PPh_3)_3$, $[RuCl_2(p\text{-cymene})]_2$, $[RuCl_2(COD)]_n$, and $RuCl_3$ in toluene at 120 °C for

Table 1 Optimization of the reaction conditions for the selective reduction of *N*-phenyl maleimide[a]

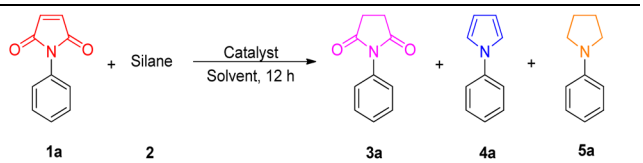

Entry	Catalyst	Silane	Solvent	Temp. (°C)	Yield (%) **3a**/**4a**/**5a**
1[b]	$RuHCl(CO)(PPh_3)_3$	H_3SiPh	Toluene	120	4/55/40
2[b]	$Ru_3(CO)_{12}$	H_3SiPh	Toluene	120	0/40/60
3[b]	$RuH_2(CO)(PPh_3)_3$	H_3SiPh	Toluene	120	9/21/64
4[b]	$[RuCl_2(p\text{-cymene})]_2$	H_3SiPh	Toluene	120	20/16/57
5[b]	$RuCl_2(PPh_3)_3$	H_3SiPh	Toluene	120	6/33/60
6[b]	$[RuCl_2(COD)]_n$	H_3SiPh	Toluene	120	31/15/47
7[b]	$RuCl_3$	H_3SiPh	Toluene	120	44/15/40
8	—	H_3SiPh	Toluene	120	0/0/0
9	$RuCl_3$@CAC	H_3SiPh	Toluene	120	14/0/0
10	$Cu(OTf)_2$@CAC	H_3SiPh	Toluene	120	97/0/0
11	$Cu(OTf)_2$@CAC	—	Toluene	120	0/0/0
12	$Cu(OTf)_2$@CAC	$HSi(Me)_2Ph$	Toluene	120	10/0/0
13	$Cu(OTf)_2$@CAC	H_2SiPh_2	Toluene	120	24/0/0
14	$Cu(OTf)_2$@CAC	$HSiEt_3$	Toluene	120	4/0/0
15	$Cu(OTf)_2$@CAC	H_3SiPh	1,4-Dioxane	100	98/0/0
16	$Cu(OTf)_2$@CAC	H_3SiPh	CH_3CN	80	16/0/0
17	$Cu(OTf)_2$@CAC	H_3SiPh	DMC	90	62/0/0
18	$Cu(OTf)_2$@CAC	H_3SiPh	THF	60	99/0/0
19[c]	$Cu(OTf)_2$	H_3SiPh	THF	60	22/0/0

[a] Reaction conditions: 1-phenyl-1*H*-pyrrole-2,5-dione **1a** (0.25 mmol), silane **2** (0.5 mmol), catalyst (20 mg, 1.2 mol%), solvent (1.0 mL) at 120 °C, 12 h, detected by GC. [b] 5 mol%. [c] 1.2 mol%.

12 h. A mixture of different ratios of products succinimide **3a**, pyrrolidine **4a**, and pyrrole **5a** was always obtained (Table 1, entries 1–7). Notably, no reaction of *N*-phenyl maleimide **1a** was detected without the additional catalyst (Table 1, entry 8). When a nanostructured $RuCl_3$-based biomass carbon aerogel catalyst ($RuCl_3$@CAC) was used instead of ruthenium complexes, only 14% yield but with highly selective product succinimide **3a** was obtained (Table 1, entry 9). However, a 97% yield of succinimide **3a** was produced by using $Cu(OTf)_2$@CAC as the catalyst (Table 1, entry 10). Different hydrosilanes (HSi$(Me)_2$Ph, H_2SiPh_2, and $HSiPh_3$) and solvents (1,4-dioxane, CH_3CN, DMC, and THF) were then evaluated, (Table 1, entries 11–18) and H_3SiPh as the hydrogen donor and THF as the solvent in the presence of the $Cu(OTf)_2$@CAC at 60 °C for 12 h were the optimized reaction conditions (Table 1, entry 18). The same catalyst loading using $Cu(OTf)_2$ just led to a 22% yield of succinimide **3a** under the above conditions (Table 1, entry 19).

With the results in Table 1, we explored the substrate scopes of this first $Cu(OTf)_2$@CAC-catalyzed selective reductions (Scheme 1). Firstly, a 1-aryl ring of maleimide-bearing substituents including –OMe, –Me, $-^tBu$, $-^iPr$, –OPh, –OH, –F, –Cl, –Br, –I, $-CF_3$, *etc*. The *ortho*, *meta*, or *para* positions (**3b–3q**) smoothly transferred to the corresponding succinimide compounds in 40–92% yields. The electronic effect and steric effects did not hinder this selective catalytic reduction. Interestingly, 1-arylmaleimides **1r–3t** with ketone and ester groups were tolerated and isolated in good yields without reducing the C=O bond in this catalytic reduction system. Moreover, succinimide with *N*-functional rings, such as benzyl, naphthalene, fluorene, pyrene, and *aminoglutethimide* (**3u–3aa**), produced good yields. Moreover, phenyl and methyl-substituted maleimide **1ab** and **1ac** would also be applied in this transformation, which could give a quaternary carbon center of the corresponding product.

To gain insight into the mechanism of this reaction, some controlled experiments were conducted (Scheme 2). No C=O bond was reduced from amide under standard conditions, whereas 4-methoxystyrene could be easily converted to 4-ethylanisole. Moreover, when 0.2 mL of D_2O was added to the reaction, deuterated compound **3ab-D** was obtained from the transformation of substrate **1ab**. These results indicated that the C=C bond is easier to reduce than the –CONR– bond. When the reaction was conducted under N_2, only 20% yield of compound **3a** was detected, but when the reaction mixture was kept under air for 5 h the yield of compound **3a** increased to 99%. Moreover, an important observation is the formation of 1,3-diphenyldisiloxane during the reaction. These results rule out the possibility that the O atom of 1,3-diphenyldisiloxane comes from the air. As Cu(0) and Cu(I) species were detected on the CAC, $Cu^{(0)}$@CAC and $Cu^{(I)}$(OTf)@CAC were prepared and tested in the model reaction and full yield of succinimide **3a** was found with $Cu^{(I)}$(OTf)@CAC, which means Cu(I) on the CAC plays an important role in this catalytic reaction.

In addition, the catalytic performance with different temperatures has been evaluated. As shown in Fig. 4, only 21% yield of succinimide **3a** was obtained and 79% yield of

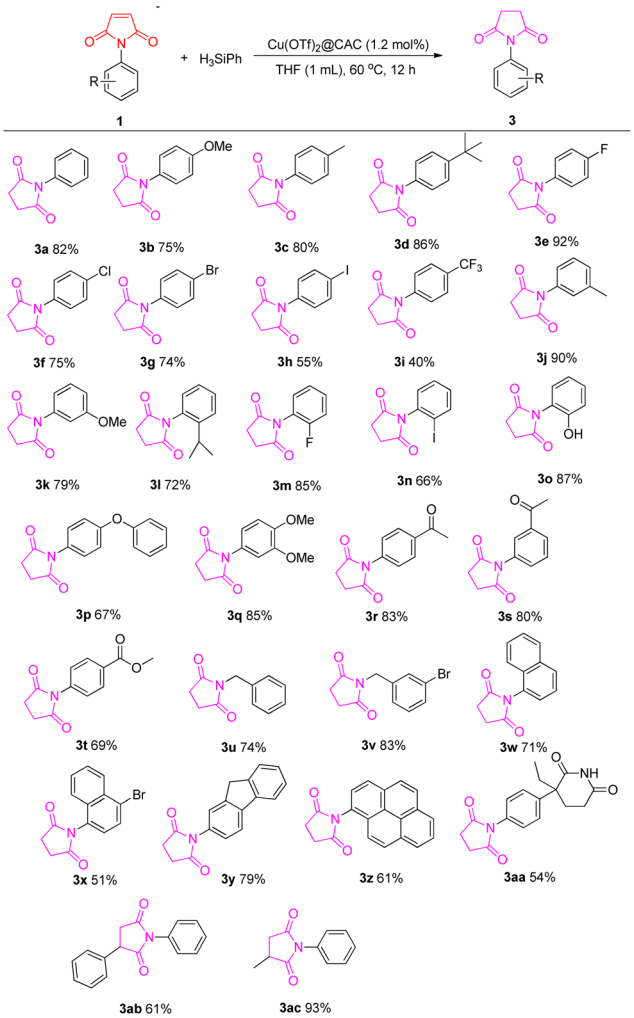

Scheme 1 $Cu(OTf)_2$@CAC catalyzed selective reduction of maleimides. Maleimide **1a** (0.5 mmol), $Cu(OTf)_2$@CAC (1.2 mol%, 20 mg), $PhSiH_3$ (1.0 mmol), THF (1 mL), at 60 °C, for 12 h.

N-phenyl maleimide **1a** was still observed. The yield of succinimide **3a** is slowly increasing below 40 °C, whereas *N*-phenyl maleimide **1a** reacts smoothly above 40 °C and leads to full conversion at 60 °C.

Furthermore, the stability and reusability of our newly developed $Cu(OTf)_2$@CAC were examined by the model reaction of *N*-phenyl maleimide **1a** with $PhSiH_3$ (Fig. 5). The $Cu(OTf)_2$@CAC could be easily reused for the next catalytic cycle through a simple filtration. As illustrated in Fig. 5, the $Cu(OTf)_2$@CAC could be reused at least 6 times, and the yield of product **3a** did not show a significant decline, which demonstrates excellent catalytic activity and reusability of the developed $Cu(OTf)_2$@CAC.

Based on the above controlled experiments and previous literature on copper catalyzed hydrosilylation,[26] a possible mechanism for the reaction is proposed in Scheme 3. Firstly, the "Cu–H" species would be easily generated by the reaction of phenylsilane to the Cu center of the CAC. Then, the "Cu–H"

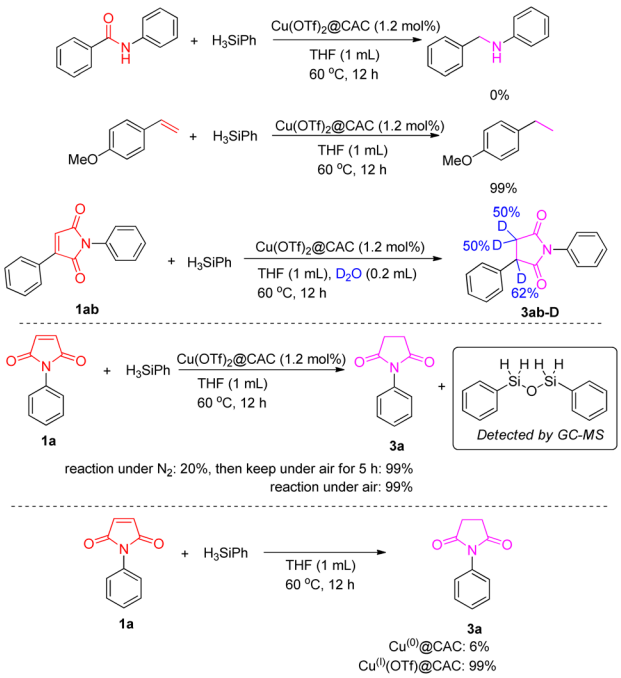

Scheme 2 Controlled experiments.

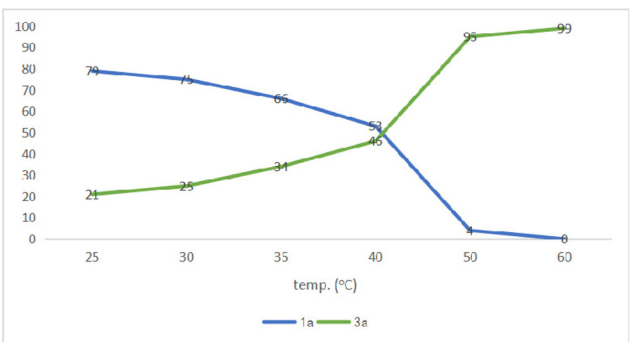

Fig. 4 The catalytic performance at different temperatures.

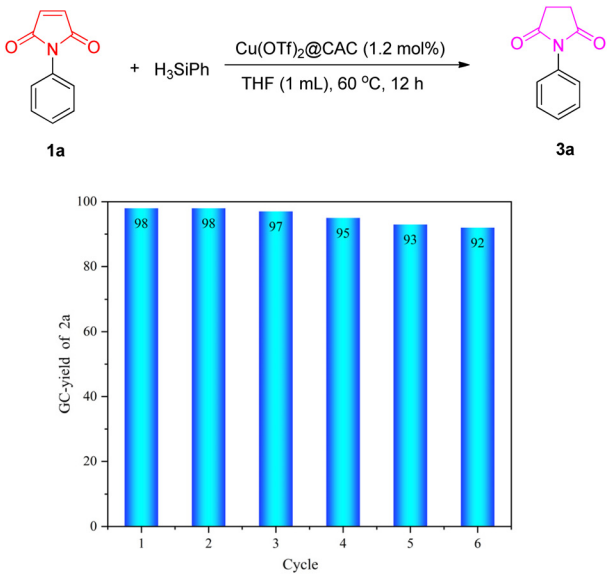

Fig. 5 Reuse of the $Cu(OTf)_2$@CAC.

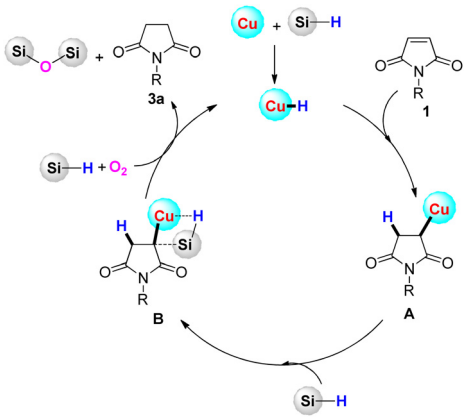

Scheme 3 Proposed mechanism for the $Cu(OTf)_2$@CAC-catalyzed selective reduction of maleimides.

species would react with maleimide **1** *via* the alkene insertion process, leading to intermediate **A**. Next, intermediate **A** underwent a σ-bond metathesis process with hydrosilane to generate intermediate **B**.[26] Finally, the desired product succinimide **3a** would be produced by the reaction of hydrosilane and oxygen from air with the release of the by-product silyl ether, and the regenerated "Cu–H" species would be used for the next cycle.

Conclusions

In summary, a novel nanostructural biomass carbon aerogel catalyst ($Cu(OTf)_2$@CAC) was designed and synthesized *via* a facile method and characterized by SEM, TEM, BET, Raman mapping, and XPS results. $Cu(OTf)_2$@CAC was applied as an efficient and highly selective heterogeneous catalyst for the selective reduction of maleimides to succinimides with hydrosilane as a hydrogen source, which is superior to other homogeneous metal catalysts. $Cu(OTf)_2$@CAC displayed excellent recyclability such that it could be reused at least six times without significant loss of activity. Further studies on this reaction mechanism and the application of the heterogeneous $Cu(OTf)_2$@CAC for other selective reduction processes are underway.

Experimental section

Materials

Chitin, potassium hydroxide, urea, *tert*-butanol, and copper trifluoromethane sulfonate ($Cu(OTf)_2$) were purchased from Aladdin Biochemical Technology Co., Ltd (Shanghai, China). Acetone and absolute ethanol were purchased from Guangzhou Chemical Reagent Co., Ltd. (Guangzhou, China).

Chitin powder purification

First, 400 g of crab shells were crushed, dispersed in 4 L of 4 wt% NaOH solution, and stirred for 8 h to remove proteins. Then, the substance was successively dispersed in 4 L of 0.3 wt% Na_2ClO (8 h, stirring, 80 °C) and the pH level of the mixture was constantly maintained by adding 7 wt% HCl to remove pigments and minerals. After repeating the above steps twice, chitin powders were obtained by drying at 50 °C.

Chitin hydrogel and chitin aerogel preparation

First, 5.26 g of chitin powders were added slowly to 100 g of 20 wt% KOH/4 wt% urea solution while stirring in the trap at −40 °C for 2 h. The turbid mixture turned into a yellow viscous chitin solution after centrifugation at 10 000 rpm and 0 °C. Then, the chitin solution was poured and cast into the home-made mold. The chitin gel was formed by immersing the mold in 1 L of absolute alcohol at −25 °C for 24 h. Finally, the transparent chitin hydrogel was cut into 2 × 2 cm chitin gel pieces.

Copper-based biomass-carbon aerogel catalyst (Cu$(OTf)_2$@CAC) preparation

First, 16 pieces of the chitin gel were dispersed in 50 mL of acetone to obtain chitin organogels, which are immersed in 50 mL of 5 wt% $Cu(OTf)_2$ acetone solution and stirred for 5 h (Fig. S4†). Subsequently, the chitin/Cu gels were washed and replaced with 50 mL of acetone and 50 mL of *tert*-butanol for 24 h, respectively. Then the chitin/Cu gels were immersed in a box filled with liquid nitrogen and the chitin/Cu aerogels were obtained by freeze-drying (Christ Alpha 2-4 LDplus, −80 °C, 0.045 atm). Finally, 120 mg of the chitin/Cu aerogels were carbonized under a nitrogen atmosphere at 250 °C (heating rate is 5 °C min^{-1} and cooling rate is 10 °C min^{-1}) for 1 h to obtain $Cu(OTf)_2$@CAC-1 h. What's more, 120 mg of the chitin/Cu aerogels were carbonized under a nitrogen atmosphere at 250 °C (heating rate is 5 °C min^{-1} and cooling rate is 10 °C min^{-1}) for 3 h to obtain $Cu(OTf)_2$@CAC-3 h, and 120 mg of the chitin/Cu aerogels were carbonized for 4 h using the same procedure to obtain $Cu(OTf)_2$@CAC-4 h. All $Cu(OTf)_2$@CAC-1 h, $Cu(OTf)_2$@CAC-3 h and $Cu(OTf)_2$@CAC-4 h samples were washed with 10 mL of acetone for 12 h and dried at 50 °C to remove impurities.

Data availability

All experimental data and detailed procedures are available in the ESI.†

Author contributions

Shaohuan Lv and Zhanhong Yuan contributed equally to this work. S. Lv performed the experiments and the data analysis. Z. Yuan and Z. Liu prepared the Cu@CAC catalysts and characterization. D. Ye designed the Cu@CAC catalysts and wrote the catalyst part in the manuscript. B. Li convinced the idea, wrote and revised the manuscript, and directed the project. J. Zheng, J. Ye, J. Li, and S. Xu provided some experimental assistance and discussed the project. F. Xie revised the manuscript.

Conflicts of interest

There are no conflicts to declare.

Acknowledgements

We are thankful for the support from the Foundation of the Department of Education of Guangdong Province (no: 2021ZDZX2045), the Foundation of Wuyi University (no: 2021WGALH06), and the Wuyi University Innovation and Entrepreneurship Project.

References

1 (*a*) E. Vitaku, D. T. Smith and J. T. Njardarson, *J. Med. Chem.*, 2014, **57**, 10257–10274; (*b*) V. Froidevaux, C. Negrell, S. Caillol, J. P. Pascault and B. Boutevin, *Chem. Rev.*, 2016, **116**, 14181–14224; (*c*) J. Mayol-Llinàs, A. Nelson, W. Farnaby and A. Ayscough, *Drug Discovery Today*, 2017, **22**, 965–969; (*d*) R. V. Jagadeesh, K. Murugesan, A. S. Alshammari, H. Neumann, J. Pohl, M.-M. Radnik and M. Beller, *Science*, 2017, **358**, 326–332; (*e*) O. I. Afanasyev, E. Kuchuk, D. L. Usanov and D. Chusov, *Chem. Rev.*, 2019, **119**, 11857–11911.

2 (*a*) M.-X. Zhao, Q. Liu, K.-M. Yu, X.-L. Zhao and M. Shi, *Org. Chem. Front.*, 2019, **6**, 3879–3884; (*b*) M. Aslam, S. Mohandoss and Y. R. Lee, *Org. Lett.*, 2021, **23**, 6206–6211.

3 E. C. Chen, N. Khuri, X. Liang, A. Stecula, H.-C. Chien, S. W. Yee, Y. Huang, A. Sali and K. M. Giacomini, *J. Med. Chem.*, 2017, **60**, 2685–2696.

4 C. Freiberg, H. P. Fischer and N. A. Brunner, *Antimicrob. Agents Chemother.*, 2005, **49**, 749–759.

5 K. Luo, Y. Bao, F. Liu, C. Xiao, K. Li, C. Zhang, R. Huang, J. Lin, J. Zhang and Y. Jin, *Eur. J. Med. Chem.*, 2019, **179**, 805–827.

6 (*a*) D. Wei and C. Darcel, *Chem. Rev.*, 2019, **119**, 2550–2610; (*b*) J. Wu, S. Tongdee, Y. Ammaiyappan and C. Darcel, *Adv. Synth. Catal.*, 2021, **363**, 3859–3865; (*c*) J. Ke, W. Liu, X. Zhu, X. Tan and C. He, *Angew. Chem., Int. Ed.*, 2021, **60**, 8744–8749; (*d*) D. Mu, W. Yuan, S. Chen, N. Wang, B. Yang, L. You, B. Zu, P. Yu and C. He, *J. Am. Chem. Soc.*, 2020, **142**, 13459–13468; (*e*) J. Y. Corey, *Chem. Rev.*, 2016, **116**, 11291–11435.

7 (*a*) H.-U. Blaser and F. Spindler, in *Handbook of homogeneous hydrogenation*, Ed. J. G. de Vries and C. J. Elsevier, Wiley-VCH, Weinheim, 2007, vol. 3, p. 1193; (*b*) W. Tang and X. Zhang, *Chem. Rev.*, 2003, **103**, 3029–3070; (*c*) J.-H. Xie, S.-F. Zhu and Q.-L. Zhou, *Chem. Rev.*, 2011,

111, 1713–1760; (*d*) M. Beller and C. Bolm, *Transition metals for organic synthesis*, Wiley-VCH, Weinheim, 2004; (*e*) V. G. Chandrashekhar, W. Baumann, M. Beller and R. V. Jagadeesh, *Science*, 2022, **376**, 1433–1441; (*f*) J. Hou, X. Han, Y. Zhang, J. Huang, J. Wang and K. Yuan, *Org. Lett.*, 2023, **25**, 5709–5713.

8 (*a*) R. O. Hutchins and M. K. Hutchins, in *Comprehensive Organic Synthesis*, ed. B. M. Trost and I. Fleming, Pergamon Press, Oxford, U. K., 1991, vol. 8, pp. 25–78; (*b*) J. Seyden-Penne, *Reductions by the Alumino and Borohydrides in Organic Synthesis*, Wiley-VCH, New York, 2nd edn, 1997, pp. 122–129.

9 (*a*) Y. Sheng, Y. Gao, B. Duan, M. Lv, Y. Chen, M. Yang, J. Zhou, G. Liang and Z. Song, *Adv. Synth. Catal.*, 2022, **364**, 307–313; (*b*) I. Dokli, R. Pohl, B. Klepetářová and U. Jahn, *Chem. Commun.*, 2019, **55**, 3931–3934.

10 (*a*) M. Ito, S. Ayaka, C. Kobayashi and T. Ikariya, *J. Am. Chem. Soc.*, 2007, **129**, 290–291; (*b*) L. Longwitz and T. Werner, *Angew. Chem., Int. Ed.*, 2020, **59**, 2760–2763.

11 (*a*) J. Li, A. Mao, W. Yao, H. Zhu and D. Wang, *Green Chem.*, 2022, **24**, 2602–2612; (*b*) J. Li, M. Yu, Z.-C. Duan, H. Zhu, W. Yao and D. Wang, *Mater. Chem. Front.*, 2021, **5**, 7861–7872; (*c*) R. Tao, Y. Yang, H. Zhu, X. Hu and D. Wang, *Green Chem.*, 2020, **22**, 8452–8461; (*d*) W.-Y. Huang, G.-Q. Wang, W.-H. Li, T.-T. Li, G.-J. Ji, S.-C. Ren, M. Jiang, L. Yan, H.-T. Tang, Y.-M. Pan and Y.-J. Ding, *Chem*, 2020, **6**, 2300–2313; (*e*) W.-H. Li, C.-Y. Li, H.-Y. Xiong, Y. Liu, W.-Y. Huang, G.-J. Ji, Z. Jiang, H.-T. Tang, Y.-M. Pan and Y.-J. Ding, *Angew. Chem., Int. Ed.*, 2019, **58**, 2448–2453; (*f*) G. Gao, J.-Q. Di, H.-Y. Zhang, L.-P. Mo and Z.-H. Zhang, *J. Catal.*, 2020, **387**, 39–46; (*g*) Y.-M. Wang, J.-B. Wang, J. Huang, Z.-S. Cui, M. Zhang and Z.-H. Zhang, *J. Catal.*, 2023, **427**, 115100.

12 (*a*) Y. Guo, S. Mei, K. Yuan, D.-J. Wang, H.-C. Liu, C.-H. Yan and Y.-W. Zhang, *ACS Catal.*, 2018, **8**, 6203–6215; (*b*) S. Navarro-Jaen, J. C. Navarro, L. F. Bobadilla, M. A. Centeno, O. H. Laguna and J. A. Odriozola, *Appl. Surf. Sci.*, 2019, **483**, 750–761; (*c*) A. Bordet, L.-M. Lacroix, P.-F. Fazzini, J. Carrey, K. Soulantica and B. Chaudret, *Angew. Chem., Int. Ed.*, 2016, **55**, 15894–15898; (*d*) M. I. Qadir, F. Bernardi, J. D. Scholten, D. L. Baptista and J. Dupont, *Appl. Catal., B*, 2019, **252**, 10–17.

13 Z. Zheng, L. Deiana, D. Posevins, A. A. Rafi, K. Zhang, M. J. Johansson, C.-W. Tai, A. Cordova and J.-E. Backvall, *ACS Catal.*, 2022, **12**, 1791–1796.

14 (*a*) H. Su, K.-X. Zhang, B. Zhang, H.-H. Wang, Q.-Y. Yu, X.-H. Li, M. Antonietti and J.-S. Chen, *J. Am. Chem. Soc.*, 2017, **139**, 811–818; (*b*) Y. X. Zhou, Y. Z. Chen, L. Cao, J. Lu and H. L. Jiang, *Chem. Commun.*, 2015, **51**, 8292–8295; (*c*) W. Zhong, H. Liu, C. Bai, S. Liao and Y. Li, *ACS Catal.*, 2015, **5**, 1850–1856; (*d*) R. V. Jagadeesh, H. Junge, M. M. Pohl, J. Radnik, A. Bruckner and M. Beller, *J. Am. Chem. Soc.*, 2013, **135**, 10776–10782; (*e*) C. Zhu, Z. Tan, H. Jiang and M. Zhang, *Green Chem.*, 2018, **20**, 1992–1997.

15 (*a*) G. Liang, A. Wang, L. Li, G. Xu, N. Yan and T. Zhang, *Angew. Chem., Int. Ed.*, 2017, **56**, 3050–3054; (*b*) G. Liang, Y. Zhou, J. Zhao, A. Y. Khodakov and V. V. Ordomsky, *ACS Catal.*, 2018, **8**, 11226–11234; (*c*) T. Komanoya, T. Kinemura, Y. Kita, K. Kamata and M. Hara, *J. Am. Chem. Soc.*, 2017, **139**, 11493–11499.

16 (*a*) M. R. Axet, S. Conejero and I. C. Gerber, *ACS Appl. Nano Mater.*, 2018, **1**, 5885–5894; (*b*) F. Leng, I. C. Gerber, P. Lecante, S. Moldovan, M. Girleanu, M. R. Axet and P. Serp, *ACS Catal.*, 2016, **6**, 6018–6024; (*c*) H. Ye, Q. Wang, M. Catalano, N. Lu, J. Vermeylen, M. J. Kim, Y. Liu, Y. Sun and X. Xia, *Nano Lett.*, 2016, **16**, 2812–2817; (*d*) M. Zhao, L. Xu, M. Vara, A. O. Elnabawy, K. D. Gilroy, Z. D. Hood, S. Zhou, L. Figueroa-Cosme, M. Chi, M. Mavrikakis and Y. Xia, *ACS Catal.*, 2018, **8**, 6948–6960; (*e*) C. Wang, R. Ciganda, L. Salmon, D. Gregurec, J. Irigoyen, S. Moya, J. Ruiz and D. Astruc, *Angew. Chem., Int. Ed.*, 2016, **55**, 3091–3095; (*f*) J.-L. Sun, H. Jiang, P. H. Dixneuf and M. Zhang, *J. Am. Chem. Soc.*, 2023, **145**(31), 17329–17336.

17 (*a*) K. Sun, H. Shan, G.-P. Lu, C. Cai and M. Beller, *Angew. Chem., Int. Ed.*, 2021, **60**, 25188–25202; (*b*) J. Sun, C. Ci, H. Jiang, P. H. Dixneuf and M. Zhang, *Angew. Chem., Int. Ed.*, 2023, e202303007; (*c*) Q. Liu, C. Ci, H. Zhao, R. Xie, H. Jiang and M. Zhang, *Green Chem.*, 2023, **25**, 678–683; (*d*) H. Jia, R. Xie, G. Lu, H. Jiang and M. Zhang, *ACS Catal.*, 2022, **12**, 10294–10303; (*e*) R. Xie, W. Mao, H. Jia, J. Sun, G. Lu, H. Jiang and M. Zhang, *Chem. Sci.*, 2021, **12**, 13802–13808.

18 (*a*) Z. Lin, J. Zou, S. Li, C. Zhang, F. Xie, B. Li and D. Ye, *ACS Sustainable Chem. Eng.*, 2021, **9**, 1568–1575; (*b*) B. Li, S. Liu, Q. Lin, Y. Shao, S. Peng and Y. Li, *Chem. Commun.*, 2018, **54**, 9214–9217; (*c*) X. Zhang, H. Liu, X. Sheng, X. Mai, S. Hou, B. Li, X. Chen, Y. Li and F. Xie, *J. Catal.*, 2022, **408**, 227–235; (*d*) F. Xie, X. Chen, X. Zhang, C. Luo, S. Lin, X. Chen, B. Li, Y. Li and M. Zhang, *J. Catal.*, 2021, **398**, 192–197.

19 P. Xi, Z. Xu, D. Gao, F. Chen, D. Xue, C.-L. Tao and Z.-N. Chen, *RSC Adv.*, 2014, **4**, 14206–14209.

20 M. Kaya, M. Mujtaba, H. Ehrlich, A. M. Salaberria, T. Baran, C. T. Amemiya, R. Galli, L. Akyuz, I. Sargin and J. Labidi, *Carbohydr. Polym.*, 2017, **176**, 177–186.

21 X. Li, L. Zhu, T. Kasuga, M. Nogi and H. Koga, *Chem. Eng. J.*, 2022, **450**, 137943.

22 H. F. Heiba, A. A. Taha, A. R. Mostafa, L. A. Mohamed and M. A. Fahmy, *Int. J. Biol. Macromol.*, 2020, **152**, 554–566.

23 T. Wang, R. Yang, N. Shi, J. Yang, H. Yan, J. Wang, Z. Ding, W. Huang, Q. Luo, Y. Lin, J. Gao and M. Han, *Small*, 2019, **15**, 1902410.

24 J. Wang, C. Liu, J. Feng, D. Cheng, C. Zhang, Y. Yao, Z. Gu, W. Hu, J. Wan and C. Yu, *J. Hazard. Mater.*, 2020, **394**, 122567.

25 Y. Xue, Y. Li, G. Luo, K. Shi, E. Liu and J. Zhou, *Adv. Energy Mater.*, 2020, **10**, 2002644.

26 (*a*) Y. Wang, Z.-L. Wang, W.-W. Ma and Y.-H. Xu, *Org. Lett.*, 2022, **24**, 4081–4086; (*b*) M. Zhang, Y. Ji, Z. Zhang and C. Zhang, *Org. Lett.*, 2022, **24**, 2756–2761; (*c*) M. W. Gribble Jr., M. T. Pirnot, J. S. Bandar, R. Y. Liu and S. L. Buchwald, *J. Am. Chem. Soc.*, 2017, **139**, 2192–2195.

